Supporting Information

Chen et al. 10.1073/pnas.1210285109

SI Text

Cluster CIMS Instrumentation. The National Center for Atmospheric Research (NCAR) Cluster chemical ionization mass spectrometer (CIMS) was described in previous publications (1, 2). The ambient Atlanta measurements described in this paper were done using that instrument. The University of Minnesota (UMN) chamber measurements were done using the UMN Cluster CIMS, which is similar in design to the NCAR Cluster CIMS but not identical. In this section, information regarding techniques used to detect neutral molecular clusters with these instruments is described. In addition, differences between the NCAR and UMN Cluster CIMS instruments are explained. This information may provide some insight as to why Jokinen et al. (3) were unable to detect neutral molecular clusters with the chemical ionization with the atmospheric pressure interface time-of-flight mass spectrometer (CI-APi-TOF), a chemical ionization instrument using NO_3^- reagent ions. Their high-resolution time-of-flight mass spectrometer allows them to clearly distinguish cluster peaks from background peaks at the same nominal mass and to measure the full range of masses. In contrast, the quadrupole mass spectrometer used in the Cluster CIMS provides only unit mass resolution and samples only selected masses. Their work led them to question Cluster CIMS measurements discussed by Zhao et al. (2) and Jiang et al. (4). The Hyytiälä measurements (3) were carried out in a relatively pristine environment where sulfuric acid vapor concentrations were typically more than an order of magnitude below values found in our chamber and Atlanta studies. The concentrations of basic gaseous compounds in Atlanta and the chamber studies (typically >1 ppbv) were also probably significantly higher than in Hyytiälä. It follows that concentrations of neutral molecular clusters in Hyytiälä would also have been at least a factor of 10 lower than for our studies. Therefore, both differences in instrumentation (described in this section) and measurement conditions likely contributed to the inability of Jokinen et al. (3) to detect neutral molecular clusters.

The measurement of neutral clusters is made difficult by the chemical complexity of the clusters themselves, their very low (typically 1 part per 10^{15}) concentrations, and the potential interferences from ion-induced clustering (IIC), ambient ion clusters, and compounds of similar mass that likely contain organic acids. It is for this reason that the Cluster CIMS is quite unique and its operation significantly altered from its OH/sulfuric acid measurement predecessor (5) that Jokinen et al. (3) reference for their own sampling technique. The ion sampling optics have been modified so as to minimize ion cluster breakup, so much so that the previously measured core ions NO_3^- and HSO_4^-, which dominated the mass spectra in the original instrument, are virtually absent in the Cluster CIMS, with HSO_4^- making up only ~1% of the $HSO_4^- + HSO_4^-HNO_3$ total. Also, for reasons described by Zhao et al. (2), a temperature-regulated cooler was used to reduce the concentration of HNO_3 vapor delivered to the ion source. Fluorine impurities have long been known to play a role in negative ion chemistry; their likely source, Teflon, could not be entirely eliminated but was minimized in the Cluster CIMS. Whereas the Cluster CIMS has only integer mass resolution, its time resolution of about 5 min allows resolution of the reactant ion and several selected cluster peaks (i.e., about 1 min for one or two peaks), as shown for the Atlanta data in *Ambient Measurements with an Emphasis on Cluster CIMS Data*. This enables tracking of the structure of plumes in real time and can also help to separate out unassociated background compounds.

Ion reaction time is also a critical parameter. The Cluster CIMS reagent ion and background ion signals are observed to decrease as reaction time is increased. Signals from clusters, however, decrease more gradually. Therefore, if a background gas and a cluster are detected at the same nominal mass, the relative contribution of the cluster increases as reaction times increase. This can be used advantageously with quadrupole mass spectrometers that operate with FWHM mass resolution of 1 amu. If ion reaction time becomes too long, however, then interference from IIC begins to dominate. The ion reaction time for ambient measurements with the NCAR Cluster CIMS is about 0.5 s, or about 4 times longer than that used in the standard OH/H_2SO_4 instrument. This reaction time can be varied depending on biogenic and/or anthropogenic backgrounds or sulfuric acid concentrations. Information about IIC can also be obtained by varying the reaction time, as discussed by Zhao et al. (2). Because of the indirect nature of the ionization used in the OH instrument, the Cluster CIMS can also provide higher ion concentration despite its longer ion reaction time and thus ultimately provide significantly more sensitivity.

The UMN Cluster CIMS (6) has a smaller pumping capacity and therefore operates at a lower sampling rate (0.083 lpm) than the NCAR instrument (0.21 lpm). Mass-dependent sensitivities for the UMN instrument were measured using the technique described by Zhao et al. (2) for the NCAR instrument. The sensitivities of the UMN and NCAR instruments have a similar functional dependence on ion mass, although the absolute sensitivity of the UMN instrument (nominally 0.04 Hz/ions cm^{-3} for the range of cluster ion masses) is lower than that for the NCAR instrument (nominally 0.2 Hz/ions cm^{-3}). Also, the ion–cluster reaction time in the UMN Cluster CIMS (~0.07 s) is about 8 times shorter than for the NCAR Cluster CIMS. Therefore, the UMN instrument is less affected by IIC.

Neutral Cluster Concentrations: Accounting for IIC and Mass-Dependent Sensitivities. Obtaining cluster concentrations from Cluster CIMS measurements requires accounting for interferences from background gases that are detected at the same nominal mass as the clusters and accounting for the effects of IIC on measured cluster ion signals (2, 7) and the mass-dependent sensitivity of the mass spectrometer (2). This section explains how cluster concentrations are determined from measurements. Background subtraction for chamber and ambient measurements is discussed in the following sections.

Cluster signals measured with the Cluster CIMS are biased high due to IIC. [For example, $HSO_4^-HNO_3$ formed by the reaction of H_2SO_4 (monomer) with the $NO_3^-HNO_3$ reactant ion subsequently reacts with H_2SO_4 to produce $HSO_4^-H_2SO_4$, thereby contributing to the signal measured at m/z 195. As shown below, similar reactions also contribute to signals at other masses where neutral clusters are detected.] Rate constants for the reactions that lead to IIC are not known with certainty, and this leads to uncertainties in reported cluster concentrations. The effect of IIC was greater for the NCAR Cluster CIMS used in Atlanta than for the UMN Cluster CIMS because the ion–molecule reaction time was about a factor of 8 longer for the NCAR instrument. As discussed below, two sets of rate constants were used for IIC corrections: "effective," and collision limited. Because collision-controlled IIC corrections lead to an upper limit for IIC, calculated cluster concentrations are lower than for the effective rate constants. In practice, the collision-controlled rate constants sometimes lead to cluster concentrations that are be-

low detection limits or even negative. When calculated concentrations are above detection limits, then the cluster concentrations calculated by both sets of rate constants are comparable. Therefore, to within measurement uncertainty, the same values for evaporation rate constants, E_{2MV} and E_3, were obtained using either the effective or collision-controlled IIC reaction rates.

The approach used for IIC corrections was originally discussed by Hanson and Eisele (7) and later by Zhao et al. (2), who included more reactions. The treatment here corrects derivational errors in the coefficient a_{ij} in Zhao et al. (2). The formation of monomer (m/z 160), dimer (m/z 195), trimer (m/z 293), tetramer (m/z 391), or higher-order ions is controlled by the following ion–molecule reactions (2):

$$H_2SO_4 + NO_3^-HNO_3 \xrightarrow{k1} HSO_4^-HNO_3 + HNO_3, \quad \textbf{[S1]}$$

$$H_2SO_4 + HSO_4^-HNO_3 \xrightarrow{k21} HSO_4^-H_2SO_4 + HNO_3, \quad \textbf{[S2]}$$

$$(H_2SO_4)_2 + NO_3^-HNO_3 \xrightarrow{k2} HSO_4^-H_2SO_4 + 2HNO_3, \quad \textbf{[S3]}$$

$$(H_2SO_4)_2 + HSO_4^-HNO_3 \xrightarrow{k31} HSO_4^-(H_2SO_4)_2 + HNO_3, \quad \textbf{[S4]}$$

$$H_2SO_4 + HSO_4^-H_2SO_4 \xrightarrow{k32} HSO_4^-(H_2SO_4)_2, \quad \textbf{[S5]}$$

$$(H_2SO_4)_3 + NO_3^-HNO_3 \xrightarrow{k3} HSO_4^-(H_2SO_4)_2 + 2HNO_3, \quad \textbf{[S6]}$$

$$(H_2SO_4)_3 + HSO_4^-HNO_3 \xrightarrow{k41} HSO_4^-(H_2SO_4)_3 + HNO_3, \quad \textbf{[S7]}$$

$$(H_2SO_4)_2 + HSO_4^-H_2SO_4 \xrightarrow{k42} HSO_4^-(H_2SO_4)_3, \quad \textbf{[S8]}$$

$$H_2SO_4 + HSO_4^-(H_2SO_4)_2 \xrightarrow{k43} HSO_4^-(H_2SO_4)_3, \quad \textbf{[S9]}$$

$$(H_2SO_4)_4 + NO_3^-HNO_3 \xrightarrow{k4} HSO_4^-(H_2SO_4)_3 + 2HNO_3. \quad \textbf{[S10]}$$

Assuming that all clusters have the same ion–molecule reaction time, the differential equations for species concentrations can be integrated to obtain the following expressions for time-dependent concentrations of $[HSO_4^-HNO_3]$, $[HSO_4^-H_2SO_4]$, $[HSO_4^-(H_2SO_4)_2]$, and $[HSO_4^-(H_2SO_4)_3]$ (the species measured at m/z 160, 195, 293, and 391, respectively):

$$\frac{[HSO_4^-(H_2SO_4)]}{[HSO_4^-HNO_3]} = \frac{(R_{195,tot} - R_{195,bkg})/S_{195}}{(R_{160,tot} - R_{160,bkg})/S_{160}} = a_{20} + a_{21}t, \quad \textbf{[S11]}$$

$$\frac{[HSO_4^-(H_2SO_4)_2]}{[HSO_4^-HNO_3]} = \frac{(R_{293,tot} - R_{293,bkg})/S_{293}}{(R_{160,tot} - R_{160,bkg})/S_{160}} = a_{30} + a_{31}t + a_{32}t^2, \quad \textbf{[S12]}$$

$$\frac{[HSO_4^-(H_2SO_4)_3]}{[HSO_4^-HNO_3]} = \frac{(R_{391,tot} - R_{391,bkg})/S_{391}}{(R_{160,tot} - R_{160,bkg})/S_{160}} = a_{40} + a_{41}t + a_{42}t^2 + a_{43}t^3, \quad \textbf{[S13]}$$

where in each case the time-dependent terms are due to IIC, R_m is the response of the mass spectrometer to ions of mass m, and S_m is the mass-dependent sensitivity given in fig. 3 of ref. 2. The subscripts "tot" and "bkg" correspond, respectively, to the total mass spectrometer signal at the indicated mass and the estimated background signals from compounds detected at the same nominal mass as the clusters. Estimates of background corrections are discussed below. The coefficients a_{ij} are

$$a_{20} = \frac{k_2}{k_1} \cdot \frac{[(H_2SO_4)_2]}{[H_2SO_4]}, \quad \textbf{[S14]}$$

$$a_{21} = \frac{1}{2} \cdot k_{21} \cdot [H_2SO_4],$$

$$a_{30} = \frac{k_3}{k_1} \cdot \frac{[(H_2SO_4)_3]}{[H_2SO_4]},$$

$$a_{31} = \frac{1}{2}\left(k_{31} + \frac{k_2}{k_1} \cdot k_{32}\right) \cdot [(H_2SO_4)_2],$$

$$a_{32} = \frac{1}{6} k_{21} \cdot k_{32} \cdot [H_2SO_4]^2,$$

$$a_{40} = \frac{k_4}{k_1} \cdot \frac{[(H_2SO_4)_4]}{[H_2SO_4]},$$

$$a_{41} = \frac{1}{2}\left(k_{41} \cdot [(H_2SO_4)_3] + \frac{k_2 \cdot k_{42}}{k_1} \cdot \frac{[(H_2SO_4)_2]^2}{[H_2SO_4]} + \frac{k_3 \cdot k_{43}}{k_1} \cdot [(H_2SO_4)_3]\right),$$

$$a_{42} = \frac{1}{6}\left(k_{21} \cdot k_{42} + k_{31} \cdot k_{43} + \frac{k_2 \cdot k_{32} \cdot k_{43}}{k_1}\right) \cdot [H_2SO_4] \cdot [(H_2SO_4)_2],$$

$$a_{43} = \frac{k_{21} \cdot k_{32} \cdot k_{43}}{24} \cdot [H_2SO_4]^3.$$

In all cases, the following rate constants were used for ion–molecule reaction rate constants:

$k_1 = 1.9 \times 10^{-9}$ cm^3·s^{-1} [experimental value; Viggiano et al. (8)];
$k_2 = 1.9 \times 10^{-9}$ cm^3·s^{-1} [collision rate; Su and Bowers (9, 10)];
$k_3 = 2.2 \times 10^{-9}$ cm^3·s^{-1} [collision rate; Su and Bowers (9, 10)];
$k_4 = 2.2 \times 10^{-9}$ cm^3·s^{-1} [collision rate; Su and Bowers (9, 10)].

Two sets of rate constants were used for IIC corrections: effective values, which predict less IIC, and collision rates, which predict an upper limit for IIC (although possibly not the upper limit). The concept of effective rate coefficients was introduced by Zhao et al. (2) to explain their observations, recognizing that the values of most of the ion–molecule clustering rate coefficients have not been measured. These values may be biased due to uncertainties in the ion–molecule reaction time and its variability, which were not measured in the field and were assumed to be constant in time and set by the sample gas flow. Some of the a_i coefficients might be self-compensating but uncertainties will lead to corresponding uncertainties in these effective rate constants. The effective rate constants used by Zhao et al. (2) and in this study are

$k_{21} = 8 \times 10^{-10}$ cm^3·s^{-1};
$k_{31} = k_{32} = k_{41} = k_{42} = k_{43} = 3 \times 10^{-10}$ cm^3·s^{-1}.

The collision-limited rate constants for IIC are (9, 10)

$k_{21} = 2 \times 10^{-9}$ cm^3·s^{-1};
$k_{31} = 1.8 \times 10^{-9}$ cm^3·s^{-1};

$k_{32} = 1.6 \times 10^{-9}$ cm^3·s^{-1};
$k_{41} = 2 \times 10^{-9}$ cm^3·s^{-1};
$k_{42} = 1.7 \times 10^{-9}$ cm^3·s^{-1};
$k_{43} = 1.5 \times 10^{-9}$ cm^3·s^{-1}.

Reaction Chamber Studies. The UMN photochemical reaction chamber is a roughly 1,000-L, climate-controlled, Teflon film batch reactor within an insulated stainless steel enclosure. The temperature of the photochemical system is controlled by using a constant-temperature circulating bath to deliver coolant to heat exchangers, which are used to control the temperature of the air as it fills the Teflon bag, and of the air that surrounds the Teflon reactor. A detailed description is given by Titcombe (6). The goal of the chamber experiments was to study nucleation in a system where sulfuric acid vapor was maintained approximately constant, whereas the concentrations of gaseous amines were varied.

Clean, humidified air is fed into the Teflon reactor with instrument sampling ports closed and the UV lights off. As the bag nears capacity, sampling ports are opened to measure background concentrations of any particles and/or gases present in the reactor before reactants are added. Toward the end of the fill time, reactant gases (SO_2, O_3, amines) are added to the bag. Upon reaching bag capacity, the fill port is shut and UV lights are turned on to initiate the reactions that lead to nucleation. The chamber is equipped with two UV lamps (36 in., GLM005, American Air & Water).

Gases and nucleated clusters are sampled through stainless steel ports that penetrate 3 cm into the bottom of the Teflon reactor. Stainless steel sample lines deliver gases and nucleated species to particle sizing and chemical characterization instrumentation located directly below the reaction chamber so as to minimize sampling losses. Nucleated particles were measured with the diethylene glycol scanning mobility particle spectrometer (DEG SMPS), whereas the UMN Cluster-CIMS and ambient pressure proton transfer mass spectrometer (AmPMS) (11) sampled clusters and basic gaseous compounds. Typical experimental run times, to half deflation, are 45 min. Experiments were done using purified air containing known amounts of water vapor, sulfur dioxide (SO_2), ozone (O_3), and later, dimethyl amine. The average SO_2 concentration for all experiments was 9 ppbv (range 7–11 ppbv) and the average relative humidity was 19% (range 6–44%). O_3, dew point, temperature, and SO_2 were measured during experiments. All experiments discussed in this paper were done at 25 °C. Clean air is generated by passing house-compressed air through coalescing filters (R26/R08-02, Wilkerson Corp.) and a pure/zero air generator (Aadco Instruments, model 737–12a). A portion of the purified air is bubbled through a 5% (by volume) solution of sulfuric acid in ultrapure water to humidify the air and scrub any residual basic gaseous compounds. The temperature of the bubbler was varied to adjust the partial pressure of water vapor in air delivered to the reactor. Residual ammonia is scrubbed from the dry airflow by a filter impregnated with sulfuric acid (sulfuric acid, 95–98%, ACS Reagent, Sigma-Aldrich). The scrubbed wet and dry pure air lines merge with gas inlet lines to carry reactant species into the reaction chamber. Each line is equipped with a ball valve and/or mass flow controller to ensure one-way flow (Mass Flo, 179A and 1479A, MKS Instruments). A portion of the scrubbed dry airflow was directed to an ozone generator capable of producing a maximum concentration of 3 ppm O_3 at a flow of 1 lpm (97-0067-01, UVP, LLC). Gaseous sulfuric acid is produced by reactions of SO_2 with OH. The OH is produced by O_3 photolysis (12) in the presence of water vapor.

The Teflon film bags used in reaction chamber experiments were cleaned before use with pure air flushes, ozone "baths," heating, and UV irradiation. New Teflon film bags were quite dirty when initially installed and thus were "baked" with clean air, O_3, and UV lights illuminated for at least 24 h. Initial tests were conducted to measure background levels of gases and/or particles in the chamber. Dark conditions (i.e., the Teflon reactor filled with clean air) showed no observable increase in either the number concentration or size of particles detected by particle sizing instrumentation. Photoactive background tests were conducted by filling the chamber with filtered air and observing particle counts with UV lights illuminated. No change was observed in particle number concentration or particle size over the course of an hour. Particle backgrounds were always checked before starting a new experiment. The reaction chamber was flushed multiple times with clean air between experiments, and either baked with O_3 or flushed overnight.

Dimethyl amine was the only basic gaseous compound that was intentionally added to the chamber, and the ammonia and amines were below detection limits (<1 pptv) in the zero air used to fill the chamber. However, various amines were detected in the chamber at levels of at least several tens of pptv whether or not they were intentionally added (protonated m/z 32+46+60+74+88). Therefore, some experiments were carried out without adding amines. Matsunaga and Ziemann (13) found that fluorinated ethylene propylene Teflon reactors store secondary organic aerosol reaction products that are released back to the chamber when it is filled with clean air. A similar process likely occurs with amines. Experiments were carried out with total concentrations of amines ranging from 0.8 to 31 ppbv. At the higher concentration, dimethyl amine was the dominant amine, whereas at lower concentrations an amine mixture was measured.

Fig. S1 and Fig. 3*A* show examples of Cluster CIMS and DEG SMPS data from an experiment with total amine concentration of 0.9 ppbv, and Figs. S2 and S3 show similar data from an experiment with a total amine concentration of 31 ppbv. Figs. S1 *Top* and S2 *Top* show raw signals from the Cluster CIMS for monomer (m/z 160), dimer (m/z 195), trimer (m/z 293), and aminated trimer (m/z 338 and 352). Symbols are omitted for measurements that were below the detection limit. Fig. S1 (*Middle* and *Bottom*) and Fig. S2 (*Middle* and *Bottom*) show cluster concentrations, respectively, after subtracting background (Bg; see Fig. S1 *Top* and Fig. S2 *Top*) and making ion-induced clustering (IIC) corrections. The effective rate constants were used to obtain the cluster signals shown in the middle, whereas the collision rate constants were used for the bottom. In principle, the collision rate constants should provide an upper limit for IIC. Therefore, the cluster concentrations shown in Figs. S1 *Bottom* and S2 *Bottom* represent lower limits.

Figs. S1 and S2 show that after the UV lights were turned on, sulfuric acid vapor concentration (m/z 160) rapidly increased to levels that remained approximately constant for the duration of the experiment. The average sulfuric acid concentration for all experiments was 2.3×10^8 cm^{-3} (range from 1.0×10^8 cm^{-3} to 3.5×10^8 cm^{-3}; SD 0.8×10^8 cm^{-3}). The behavior of neutral molecular clusters, however, differed markedly for the lower and higher amine experiments. For the lower amine experiment (Fig. S1), cluster concentrations reached peak values early in the experiment and mostly dropped below detection levels (except possibly for dimer) after about 15 min. For the higher amine experiment (Fig. S2), concentrations of the dimer (195) and trimer (293) reached peak values early in the experiment before stabilizing as time progressed. Concentrations of the aminated clusters (338 and 352) reached peak values shortly after the lights were turned on and then decreased steadily, dropping below detection levels later in the experiment. The amines that were measured with the AmPMS did not decrease appreciably during the experiments, so the disappearance of the aminated clusters was not due to depletion of those gases.

Fig. 3*A* and Fig. S3 show number distributions extending from monomer (m/z 160) at the smallest size up to about 9 nm, the upper limit for the DEG SMPS. The approach used to convert cluster concentrations to number distributions is discussed by Jiang et al. (4). The time-dependent number distributions for the

lower (Fig. 3*A*) and higher (Fig. S3) amine experiments are markedly different. In both cases, number distributions increase sharply with decreasing size below 1 nm. This behavior is similar to theoretical predictions for collision-controlled nucleation (fig. 3 of ref. 14) and fig. 1a of ref. 15). However, for the lower amine experiments, clusters and particles in the ~1–1.5-nm size range drop below detection limits after about 20 min (Fig. 3*A*), whereas they remain above detection limits through the duration of the high amine experiment (Fig. S3). This implies that nucleation rates were significantly higher in the higher amine experiments.

We considered the possibility that ion clusters sampled from the chamber contributed significantly to the ions sampled by the Cluster CIMS in the chamber experiments and concluded that this is unlikely. McMurry and Rader (16) measured wall loss rates as a function of size for neutral and charged particles, and found that charged particles are lost much faster (50× at 100 nm) than neutrals. Loss rates of charged particles smaller than 100 nm were too fast to measure. Extrapolating the theoretical model from that study to smaller sizes leads to first-order loss rates for 1-nm ions of 1–10 s^{-1}. Assuming an ion production rate of ~30 $cm^{-3}{\cdot}s^{-1}$, which is near the upper bound for ion production rates in the atmosphere, estimated steady-state ion concentrations would be around 3–30 cm^{-3}. The measured sensitivity of the UMN Cluster CIMS is about 0.04 Hz/ions cm^{-3}. An ion concentration of 30 cm^{-3} would produce a signal of about 1 Hz. Measured signals are at least a factor of 20 higher than this.

Ambient Measurements with an Emphasis on Cluster CIMS Data. In addition to the chamber data described in *Reaction Chamber Studies*, ambient measurements obtained in Atlanta during the summer of 2009 were used to develop the acid–base reaction model for nucleation. Also, measurements carried out downwind of Mexico City during the 2006 Megacity Initiative: Local and Global Research Observations campaign were used to compare measured nucleation rates with values predicted by the acid–base reaction model. The field studies in Mexico City (2006) and Atlanta (2002 and 2009) have been described in previous publications (4, 17–25). This section summarizes aspects of those studies that are especially germane to this paper.

Ammonia was measured during the Mexico City field campaign (26) using a quantum cascade laser infrared absorption spectrometer similar to that described by Kolb et al. (27). Also, particle size distributions down to 3 nm were measured (18). Measurements of 8–10-nm particle composition showed that amines accounted for about 50% of the ion signal detected with the thermal desorption CIMS (28). Those observations led to our focus on amines as likely participants in nucleation in the Atlanta (2009) and chamber (2010) studies.

We organized the Nucleation and Cloud Condensation Nuclei campaign (NCCN) to investigate mechanisms of neutral nucleation at the Jefferson Street site in Atlanta (29), which is regularly impacted by plumes from several nearby coal-fired power plants (30). Measurements were carried out from mid-July through August 2009, and included measurements with the NCAR Cluster CIMS and an SMPS (31) operated with a DEG condensation particle counter (32) that allows measurements of aerosol number distributions down to 1 nm (33). This system is referred to as the DEG SMPS. Jiang et al. (4) showed that number distributions measured in Atlanta by the DEG SMPS and the Cluster CIMS were in reasonable agreement (typically a factor of 2–5) in the ~1-nm size range where they overlap. More examples of such number distributions for chamber experiments are shown in *Reaction Chamber Studies* and in this section (Atlanta measurements). As with the chamber experiments, the AmPMS (11) was used to measure amines during NCCN. The citric acid denuder difference method using chemiluminescence detection was used for ammonia (34).

During NCCN, Cluster CIMS measurements were carried out on 27 d, from July 21, 2009–August 25, 2009. On 15 of the days when Cluster CIMS measurements were obtained, SO_2 concentrations did not extend above 10 ppbv, and nucleation events were relatively weak. On those days, monomer (*m/z* 160) and dimer (*m/z* 195) were detected, but trimer and tetramer were not clearly above detection limits. On the remaining 12 d, SO_2 concentrations reached levels of 20–50 ppbv during plume impact, and trimer and tetramer were detected. Our analyses focus on those plume-impact periods. Concentrations of basic gaseous compounds (ammonia plus amines) typically exceeded 1 ppbv during these studies. Ammonia concentrations were typically about 10 times higher than the total concentration of all amines.

Fig. S4 illustrates the approach used to correct the ambient data for background. These data were obtained on August 3, 2009, when significant plume impact occurred between 1200 and 1600 hours and after 1730 hours. (Fig. S4 *Top*) Measured signal at *m/z* 166, which is likely an organic acid (possibly malonic acid), follows a smooth diurnal pattern, reaching a peak value near midday. In contrast to the monomer, dimer, and to a lesser extent trimer and tetramer, the data for *m/z* 166 are not correlated with plume impact. To estimate backgrounds which are most likely of organic or biogenic origin, we fit a lognormal curve through the normalized (with respect to the reagent ion signal at *m/z* 125) signals for *m/z* 166 and then assume that backgrounds for cluster masses follow a similar temporal trend, as shown by the solid red lines in Fig. S4. The lognormal function, used because it provided a reasonable fit to the data, is given by

$$Background = SF^{*}\left(y_0 + A\cdot\exp(-\ln(x/x_0)/width)^2\right). \quad \textbf{[S15]}$$

The constants y_0, A, and x_0 and the mass-dependent scaling factor *SF* varied somewhat from day to day, and separate fits were obtained for each day when plume impact occurred. Cluster signals are obtained by subtracting those backgrounds from measurements.

Figs. S5–S8 show examples of data from August 3, 7, and 23, 2009. The elevated values of $[SO_2]$ shown in Figs. S5 *Top*, S7 *Top*, and S8 *Top* occur during plume impact. Vertical red lines are drawn through peak values of $[SO_2]$ to guide the eye. Figs. S5*A*, S7*A*, and S8*A* also show raw signals for cluster CIMS measurements of monomer and clusters, before background subtraction. Figs. S5*B*, S7*B*, and S8*B* and Figs. S5*C*, S7*C*, and S8*C* show measured cluster concentrations obtained after background subtraction, IIC corrections, and mass-dependent sensitivity corrections. These results were obtained using effective values for IIC rate constants (Figs. S5*B*, S7*B*, and S8*B*) and collision-controlled rate constants (Figs. S5*C*, S7*C*, and S8*C*). Use of the collision-rate values of rate constants occasionally led to reported concentrations that were below detection limits or even negative, as can be seen in Figs. S5*C*, S7*C*, and S8*C*, and sometimes led to tetramer concentrations that exceeded trimer concentrations, as seen in Figs. S7 and S8. The effective rate constant proposed by Zhao et al. (2) appears to lead to more plausible results for at least some experimental sampling conditions. Contour plots (Figs. S5 *Bottom*, S7 *Bottom*, and S8 *Bottom*) of aerosol number distributions obtained by combining the data from three SMPS instruments: the DEG SMPS, a Nano SMPS, and a conventional (long-column differential mobility analyzer) SMPS. The data in Figs. S5, S7, and S8 show a clear association between measured dimer, trimer, and sometimes tetramer concentrations and elevated $[SO_2]$.

Fig. S6 compares number distributions measured with the Cluster CIMS and DEG SMPS on August 3, 2009, for nearly simultaneous measurements inside and outside the plume. There are two differences between the number distributions shown here and those published earlier for August 7 and 23 (4). First, dimer concentrations are shown in Fig. S6. The earlier work did not include dimer concentrations because of uncertainties about the IIC correction. Second, results are shown for cluster concentrations calculated using both the effective and collision rate constants for IIC.

IIC corrections were only done using the effective rate constants in the earlier work. For the August 3 and 7 number distributions, qualitatively similar results were obtained for both approaches to IIC. For August 23, dimer and trimer (but not tetramer) dropped below the detection limit when the collision rate constants were used (Fig. S8). It is implausible that tetramer was present but smaller clusters were not, so we infer from these results that the collision rate constants overpredict IIC. Clearly, better information on values for these rate constants is needed.

Note that the raw signals for the Cluster CIMS often exceeded 1000 Hz for dimer and 100 Hz for trimer and tetramer. The sensitivity of the NCAR Cluster CIMS at these masses is about 0.2 Hz/ion cm^{-3} (2). If the measured signals were due entirely to naturally charged clusters from the atmosphere rather than those formed by chemical ionization, then their concentrations would have been nominally 5,000 cm^{-3} and 500 cm^{-3}. Although we did not measure ion concentrations in Atlanta in 2009, we did measure them using the Inclined Grid Mobility Analyzer (35) in 2002 and found that total concentrations of small ions are typically less than 500 cm^{-3}. These ions cover a spectrum of sizes, whereas the Cluster CIMS detects clusters at a selected mass, so the concentration of mass-selected ions would have been less than 500 cm^{-3}. Therefore, Cluster CIMS signals in Atlanta were at least a factor of 10 higher than could be explained by naturally charged clusters assuming that they were sampled with 100% efficiency, which is unlikely.

Sub-3-nm Growth Rates in Atlanta. Kuang et al. (19) discussed the use of number distributions measured with the DEG SMPS to infer growth rates for sub-3-nm particles. These growth rates provide information that supports conclusions from the Cluster CIMS measurements used to develop the model. Kuang et al. (19) define the "growth rate enhancement factor" Γ as

$$\Gamma(D_p,t)=\frac{\text{Measured growth rate at a specified size and time}}{\text{Growth rate due to sulfuric acid condensation at the same size and time}}.$$

$\Gamma(D_p,t)$ must be at least equal to unity if monomer uptake is collision controlled. As was argued by Kuang et al. (19), the Atlanta data show that monomer uptake could be collision controlled for particles as small as 1 nm. A spherical 1-nm ammonium sulfate particle (density assumed equal to bulk density, 1769 kg/m^3), would contain about four ammonium sulfate molecules, so this result supports the argument that monomer uptake by tetramer could be collision controlled.

We have altogether 34 measurements of $\Gamma(D_p,t)$ from the 2009 NCCN study in Atlanta, on July 25 and August 7, 12, 22, and 23. We found that, to within experimental uncertainty, $1 \le \Gamma(1\text{ nm}) \le 3$ for 5/6 measurements on July 25, 3/10 measurements on August 7, 3/7 measurements on August 12, 7/7 measurements on August 22, and 1/4 measurements on August 23. In the remaining cases, $0.3 \le \Gamma(1\text{ nm}) \le 0.7$. For several of the cases where $0.3 \le \Gamma(1\text{ nm}) \le 0.7$, $\Gamma(D_p)$ asymptotically approached 1 as particle sizes approached 3–5 nm. Therefore, whereas our model is based on the argument that $\Gamma > 1$ for particles as small as 1 nm, this was not always observed, and deviations from this assumption might explain some of the scatter that is observed in ambient observations of nucleation rates. Using other techniques, different studies have also shown that $\Gamma > 1$ for sub-3-nm particles (36–39).

Model Derivation. The proposed acid–base reaction mechanism for nucleation follows the pathway illustrated by the arrows in Fig. 4. The MV dimer is assumed to be in equilibrium with the monomer:

$$A_1 + A_1 \underset{E_{2MV}}{\overset{k_{11}}{\rightleftarrows}} A_{2MV}. \qquad \textbf{[S16]}$$

Once formed, the MV dimer reacts with some other gas at the collision rate k'_{21} to form A_{2LV}:

$$A_{2MV} + B \xrightarrow{k'_{21}} A_{2LV} \qquad \textbf{[S17]}$$

In this study we assume that "other gas" is a base (ammonia or amines). The concentration of A_{2MV} is governed by

$$\frac{d[A_{2MV}]}{dt} = \frac{1}{2}k_{11}\cdot[A_1]\cdot[A_1] - E_{2MV}\cdot[A_{2MV}] - k'_{21}\cdot[A_{2MV}]\cdot[B] - [A_{2MV}]\cdot\kappa'_2, \qquad \textbf{[S18]}$$

where κ'_2 is the first-order loss rate of $A_{2\,MV}$ to larger clusters and particles, which is assumed to be collision limited and is evaluated from measured size distributions using the following expression:

$$\kappa'_2 = \kappa_2 - k_{21}\cdot[A_1], \qquad \textbf{[S19]}$$

where

$$\kappa_2 = k_{21}\cdot[A_1] + k'_{22}\cdot[A_{2MV}] + k_{22}\cdot[A_{2LV}] + \sum_{i=3}^{\infty} k_{2i}\cdot[A_i] \approx k_{21}\cdot[A_1] + \frac{\bar{c}}{4}A_{Fuchs}, \qquad \textbf{[S20]}$$

and A_{Fuchs} is the transition regime-corrected aerosol surface area (eq. 6 of ref. 40). For the Atlanta study, the summation expression was used to evaluate all κ_i values using measured aerosol size distributions. For the chamber study A_{Fuchs} was calculated using the self-preserving surface area described by McMurry and Friedlander (41). It follows from Eq. **S18** that the steady-state concentration of A_{2MV} is

$$[A_{2MV}] = \frac{1}{E_{2MV} + k'_{21}\cdot[B] + \kappa'_2}\cdot\frac{1}{2}k_{11}\cdot[A_1]\cdot[A_1]. \qquad \textbf{[S21]}$$

We assume that the A_{2MV} reacts with B to produce less volatile dimer, A_{2LV}, whose concentration is governed by

$$\frac{d[A_{2LV}]}{dt} = k'_{21}\cdot[A_{2MV}]\cdot[B] - [A_{2LV}]\cdot\kappa_2 + E_3\cdot[A_3]. \qquad \textbf{[S22]}$$

Under typical conditions, $E_3\cdot[A_3] \ll k'_{21}\cdot[A_{2MV}]\cdot[B]$, so the steady-state concentration of A_{2LV} can be approximated as

$$[A_{2LV}] \approx \frac{k'_{21}\cdot[B]}{\kappa_2}\cdot[A_{2MV}] = \frac{k'_{21}\cdot[B]}{\kappa_2}\cdot\frac{1}{E_{2MV} + k'_{21}\cdot[B] + \kappa'_2}\cdot\frac{1}{2}k_{11}\cdot[A_1]\cdot[A_1]. \qquad \textbf{[S23]}$$

All dimers are assumed to contribute to the signal measured at mass 195:

$$[A_2] = [A_{2MV}] + [A_{2LV}] \approx [A_{2LV}]. \quad \textbf{[S24]}$$

As shown in Fig. 2*A*, the measured trimer concentration is about a factor of 8 lower than the value calculated assuming that the monomer reacts with the dimer at the collision rate. Evaporation of monomer from trimer is assumed to explain these low trimer concentrations. The population balance equation for trimers is then

$$\frac{d[A_3]}{dt} = k_{21} \cdot [A_1] \cdot [A_{2LV}] - [A_3] \cdot \kappa_3 - E_3 \cdot [A_3] \quad \textbf{[S25]}$$

where

$$\kappa_3 \approx k_{31} \cdot [A_1] + \frac{\bar{c}}{4} A_{Fuchs} \quad \textbf{[S26]}$$

and the steady-state trimer concentration is

$$[A_3] = \frac{k_{21} \cdot [A_1] \cdot [A_{2LV}]}{\kappa_3 + E_3} \quad \textbf{[S27]}$$

Eqs. **S23**, **S24**, and **S27**, respectively, show the dependence of measured dimer and trimer concentrations on the evaporation rate constants E_{2MV} and E_3. These evaporation rate constants were found by fitting those expressions to data shown in Fig. 2 *A* and *B*. Fig. S9 *A* and *B* show comparisons of measurement and the model for dimer and trimer with the best-fit values of the evaporation rate constants: $E_{2MV} = 400\ s^{-1}$ (range 100–1,000 s^{-1}) and $E_3 = 0.4 \pm 0.3\ s^{-1}$. The modeled results for A_2 from Atlanta (2009) in Fig. S9*A* were calculated using both total amines and total amine plus ammonia. The modeled results are consistent with observations only when ammonia is included. Therefore, in comparing the nucleation model developed in this paper with observed ambient nucleation rates, we have used the total measured base concentration (ammonia + amines). As was mentioned in *Ambient Measurements with an Emphasis on Cluster CIMS Data*, to within measurement uncertainty the same values of E_{2MV} and E_3 were obtained when IIC corrections were made using either the effective or the collision-controlled rate constants. The data shown in black in Fig. S9*B* were all measured when monomer concentrations were below 3×10^7 molecules cm^{-3}. We did not use those data when evaluating E_3 because we suspect that with those measurements, the higher relative contributions of background led to overestimates of cluster concentrations. Including those results would not have led to a significant difference in the value of E_3.

Because the Cluster CIMS (Fig. 2*A*) and growth rate data suggest that evaporation does not occur for tetramer and larger clusters, it follows that the nucleation rate is equal to the rate at which tetramer is produced:

$$\begin{aligned} J_4 &= k_{31} \cdot [A_1] \cdot [A_3] \\ &= \left\{ \frac{k'_{21} \cdot [B]}{E_{2MV} + k'_{21} \cdot [B] + \kappa'_2} \cdot \frac{k_{21} \cdot [A_1]}{\kappa_2} \cdot \frac{k_{31} \cdot [A_1]}{\kappa_3 + E_3} \right\} \\ &\quad \cdot \frac{1}{2} k_{11} \cdot [A_1] \cdot [A_1] \\ &= P \cdot \frac{1}{2} k_{11} \cdot A_1 \cdot A_1, \end{aligned} \quad \textbf{[S28]}$$

where the prefactor P is less than 1. For very high monomer concentrations ($[A_1] > 10^9\ cm^{-3}$), P is insensitive to $[A_1]$ because $k_{21}[A_1]$ and $k_{31}[A_1]$ dominate the values of κ_2 and κ_3. As monomer concentrations decrease, P tends to increase with $[A_1]$.

Errors in Measured Cluster Concentrations. A root sum of squares (RSS) analysis was applied to Eqs. **S11–S13** to estimate the systematic errors in measured dimer ($[HSO_4^-(H_2SO_4)]$), trimer ($[HSO_4^-(H_2SO_4)_2]$), and tetramer ($[HSO_4^-(H_2SO_4)_3]$) concentrations. Table S1 summarizes assumptions made about variable uncertainties when carrying out these estimates. The basis for the estimated uncertainties in monomer concentration ($[HSO_4^-HNO_3]$), reaction time, and mass-dependent sensitivities is discussed by Zhao et al. (2). Estimates for uncertainties in background signals for dimer, trimer, and tetramer are based on the approach used for background correction discussed earlier in the *SI Text*, and reflect educated guesses based on observed variabilities in signals. Based on arguments given in the paper, we infer that the loss of H_2SO_4 from dimer, trimer, and tetramer does not occur to any significant extent, and is likely negligible relative to other uncertainties. Tabulated uncertainties in association rate constants reflect the range of values used in the IIC corrections discussed above. Calculated overall RSS systematic uncertainties for dimer, trimer, and tetramer are shown in the bottom row of Table S1.

Measurements of cluster concentrations are also affected by random errors. The scatter in the data shown in Fig. 2 is likely due partly to random error and partly to variations in concentrations of unmeasured reactive trace gases that affect cluster concentrations. Estimated random errors are roughly equal to the systematic errors tabulated in Table S1. The overall uncertainty in concentrations of monomer, dimer, trimer, and tetramer, obtained by combining the systematic and random errors, are estimated to be factors of 1.5, 3, 5, and 5, respectively. Some information on measurement uncertainties can also be inferred by comparing independent measurements by the DEG SMPS and Cluster CIMS at the same nominal size. Although discrepancies exceeding a factor of 10 are sometimes observed, most measurements agree to within a factor of 3 to 5, consistent with the result from error propagation analysis for Cluster CIMS measurements. Better estimates of accuracy will require better calibrations than are currently possible.

1. Zhao J, et al. (2011) Observation of neutral sulfuric acid-amine containing clusters in laboratory and ambient measurements. *Atmos Chem Phys* 11:10823–10836.
2. Zhao J, Eisele FL, Titcombe M, Kuang C, McMurry PH (2010) Chemical ionization mass spectrometric measurements of atmospheric neutral clusters using the cluster-CIMS. *J Geophys Res* 115:D08205.
3. Jokinen T, et al. (2012) Atmospheric sulphuric acid and neutral cluster measurements using CI-APi-TOF. *Atmos Chem Phys* 12:4117–4125.
4. Jiang J, et al. (2011) First measurements of atmospheric cluster and 1-2 nm particle number distributions during nucleation events. *Aerosol Sci Technol* 45:ii–v.
5. Eisele FL, Tanner DJ (1993) Measurement of the gas phase concentration of H_2SO_4 and methane sulfonic acid and estimates of H_2SO_4 production and loss in the atmosphere. *J Geophys Res* 98:9001–9010.
6. Titcombe M (2012) New particle formation: Sulfuric acid and amine chemical nucleation. PhD dissertation (Univ. of Minnesota, Minneapolis, MN).
7. Hanson DR, Eisele FL (2002) Measurement of prenucleation molecular clusters in the NH_3, H_2SO_4, H_2O system. *J Geophys Res, [Atmos]* 107(D12):4158.
8. Viggiano AA, Seeley JV, Mundis PL, Williamson JS, Morris RA (1997) Rate constants for reactions of $XO_3^-(H_2O)_n$ (X=C, HC, and N) and $NO_3^-(HNO_3)_n$ with H_2SO_4: Implications for atmospheric detection of H_2SO_4. *J Phys Chem A* 101:8275–8278.
9. Su T, Bowers MT (1973) Theory of ion-polar molecule collisions: Comparison with experimental charge-transfer reactions of rare-gas ions to geometric isomers of difluorobenzene and dichloroethylene. *J Chem Phys* 58(7):3027–3037.
10. Su T, Bowers MT (1973) Ion-polar molecule collisions: Effect of molecular size on ion-polar molecule rate constants. *J Am Chem Soc* 95(23):7609–7610.
11. Hanson DR, McMurry PH, Jiang J, Tanner D, Huey LG (2011) Ambient pressure proton transfer mass spectrometry: Detection of amines and ammonia. *Environ Sci Technol* 45(20):8881–8888.
12. Seinfeld JH, Pandis SN (1998) *Atmospheric Chemisry and Physics: From Air Pollution to Climate Change* (Wiley Interscience, New York).
13. Matsunaga A, Ziemann PJ (2010) Gas-wall partitioning of organic compounds in Teflon film chamber and potential effects on reaction product and aerosol yield measurements. *Aerosol Sci Technol* 44:881–892.

14. McMurry PH (1980) Photochemical aerosol formation from SO2: A theoretical analysis of smog chamber data. *J Colloid Interface Sci* 78:513–527.
15. Rao NP, McMurry PH (1989) Nucleation and growth of aerosol in chemically reacting systems. *Aerosol Sci Technol* 11:120–132.
16. McMurry PH, Rader DJ (1985) Aerosol wall losses in electrostatically charged chamber. *Aerosol Sci Technol* 4:249–268.
17. Smith JN, et al. (2008) Chemical composition of atmospheric nanoparticles formed from nucleation in Tecamac, Mexico: Evidence for an important role for organic species in nanoparticle growth. *Geophys Res Lett* 35(4):L04808.
18. Iida K, Stolzenburg MR, McMurry PH, Smith JN (2008) Estimating nanoparticle growth rates from size-dependent charged fractions: Analysis of new particle formation events in Mexico City. *J Geophys Res, [Atmos]* 113(D5):D05207.
19. Kuang C, et al. (2012) Size and time-resolved measurements of 1 to 5 nm freshly formed atmospheric nuclei. *Atmos Chem Phys* 12:3573–3589.
20. Smith JN, et al. (2005) Chemical composition of atmospheric nanoparticles during nucleation events in Atlanta. *J Geophys Res, [Atmos]* 110(D22):D22S03.
21. McMurry PH, et al. (2005) A criterion for new particle formation in the sulfur-rich Atlanta atmosphere. *J Geophys Res, [Atmos]* 110(D22):D22S02.
22. Stolzenburg MR, et al. (2005) Growth rates of freshly nucleated atmospheric particles in Atlanta. *J Geophys Res, [Atmos]* 110(D22):D22S05.
23. Sakurai H, et al. (2005) Hygroscopicity and volatility of 4-10 nm particles during summertime atmospheric nucleation events in urban Atlanta. *J Geophys Res* 110(D22):D22S04.
24. McMurry PH, Eisele FL (2005) Preface to topical collection on new particle formation in Atlanta. *J Geophys Res, [Atmos]* 110(D22):D22S01.
25. Fountoukis C, et al. (2009) Thermodynamic characterization of Mexico City aerosol during MILAGRO 2006. *Atmos Chem Phys* 9(6):2141–2156.
26. Molina LT, et al. (2010) An overview of the MILAGRO 2006 Campaign: Mexico City emissions and their transport and transformation. *Atmos Chem Phys* 10:8697–8760.
27. Kolb CE, et al. (2004) Mobile laboratory with rapid response instruments for real-time measurements of urban and regional trace gas and particulate distributions and emission source characteristics. *Environ Sci Technol* 38(21):5694–5703.
28. Smith JN, et al. (2010) Observations of aminium salts in atmospheric nanoparticles and possible climatic implications. *Proc Natl Acad Sci USA* 107(15):6634–6639.
29. Solomon PA, et al. (2003) Overview of the 1999 Atlanta Supersites Project. *J Geophys Res, [Atmos]* 108:8413.
30. Woo KS, Chen DR, Pui DYH, McMurry PH (2001) Measurement of Atlanta aerosol size distributions: Observations of ultrafine particle events. *Aerosol Sci Technol* 34(1):75–87.
31. Wang SC, Flagan RC (1990) Scanning electrical mobility spectrometer. *Aerosol Sci Technol* 13:230–240.
32. Iida K, Stolzenburg MR, McMurry PH (2009) Effect of working fluid on sub-2 nm particle detection with a laminar flow ultrafine condensation particle counter. *Aerosol Sci Technol* 43(1):81–96.
33. Jiang J, Chen M, Kuang C, Attoui M, McMurry PH (2011) Electrical mobility spectrometer using a diethylene glycol condensation particle counter for measurements of aerosol size distributions down to 1 nm. *Aerosol Sci Technol* 45:510–521.
34. Saylor RD, Edgerton ES, Hartsell BE, Baumann K, Hansen DA (2010) Continuous gaseous and total ammonia measurements from the southeastern research and characterization (SEARCH) study. *Atmos Environ* 44:4994–5004.
35. Tammet H (2003) *Inclined Grid Mobility Analyzer: The Plan Model* (International Aerosol Research Assembly, Taipei, Taiwan).
36. Weber RJ, et al. (1997) Measurements of new particle formation and ultrafine particle growth rates at a clean continental site. *J Geophys Res* 102(D4):4375–4385.
37. Weber RJ, et al. (1998) A study of new particle formation and growth involving biogenic trace gas species measured during ACE-1. *J Geophys Res* 103(D13): 16385–16396.
38. Fiedler V, et al. (2005) The contribution of sulphuric acid to atmospheric particle formation and growth: A comparison between boundary layers in Northern and Central Europe. *Atmos Chem Phys* 5:1773–1785.
39. Sihto SL, et al. (2006) Atmospheric sulphuric acid and aerosol formation: Implications from atmospheric measurements for nucleation and early growth mechanisms. *Atmos Chem Phys* 6:4079–4091.
40. McMurry PH (1983) New particle formation in the presence of an aerosol: Rates, time scales and sub-0.01 μm size distributions. *J Colloid Interface Sci* 95(1):72–80.
41. McMurry PH, Friedlander SK (1977) Aerosol formation in reacting gases: Relation of surface area to rate of gas-to-particle conversion. *J Colloid Interface Sci* 64(2): 248–257.

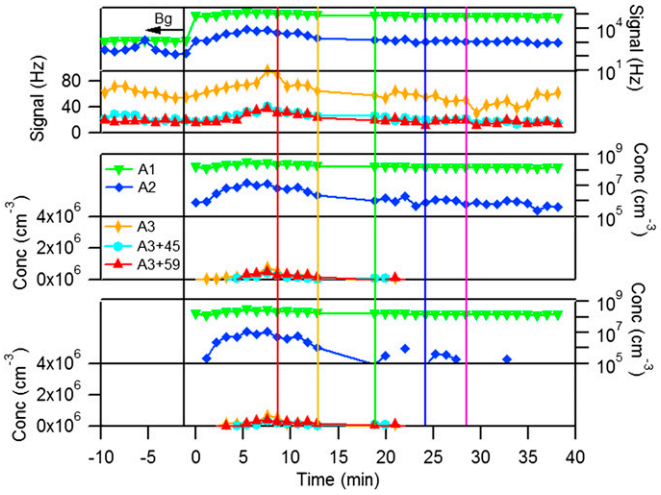

Fig. S1. Cluster CIMS time series measurements for chamber experiment 2, July 13, 2010 [(total amine) = 0.9 ppbv]. (*Top*) Signals (Hz) for *m/z* 160, 195, 293, 338, and 352. (*Middle* and *Bottom*) Measured cluster concentrations after correcting for Bg and ion induced clustering. (*Middle*) Effective rate constants were used. (*Bottom*) Collision rate constants were used. Symbols are omitted for signals below the detection limit.

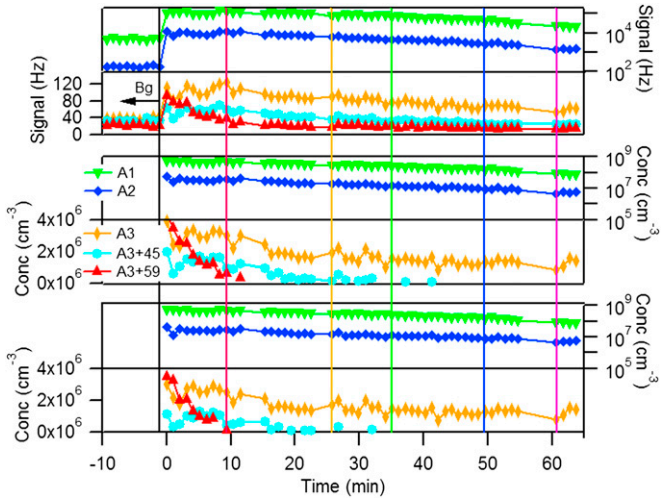

Fig. S2. Cluster CIMS time series measurements for experiment 3, July 27, 2010 [(total amine) = 0.9 ppbv]. (*Top*) Signals (Hz) for *m/z* 160, 195, 293, 338, and 352. (*Middle* and *Bottom*) Measured cluster concentrations after correcting for Bg and IIC. (*Middle*) Effective rate constants were used. (*Bottom*) Collision rate constants were used. Symbols are omitted for signals below the detection limit.

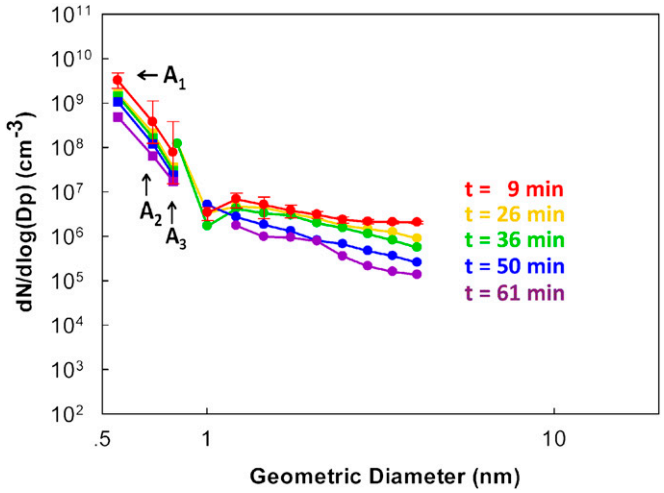

Fig. S3. Number distributions obtained from "■," Cluster CIMS; (●) DEG SMPS for experiment 3, July 27, 2010 [(total amine) = 31 ppbv].

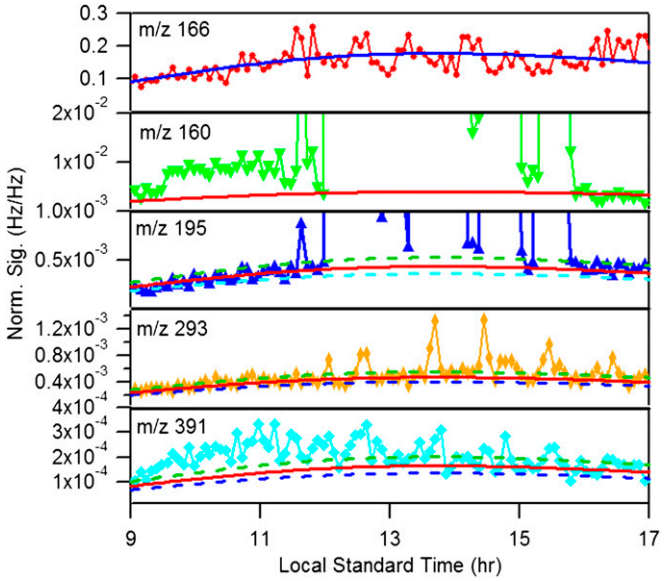

Fig. S4. Cluster CIMS signals on August 3, 2009 (Atlanta). (*Top*) Lognormal fit to *m/z* 166 measurements, likely an organic acid (possibly malonic acid). The four bottom red curves show estimated backgrounds for cluster signals obtained by scaling the malonic acid fit to signals measured early and late in the day. The dashed lines show estimated uncertainties in background corrections.

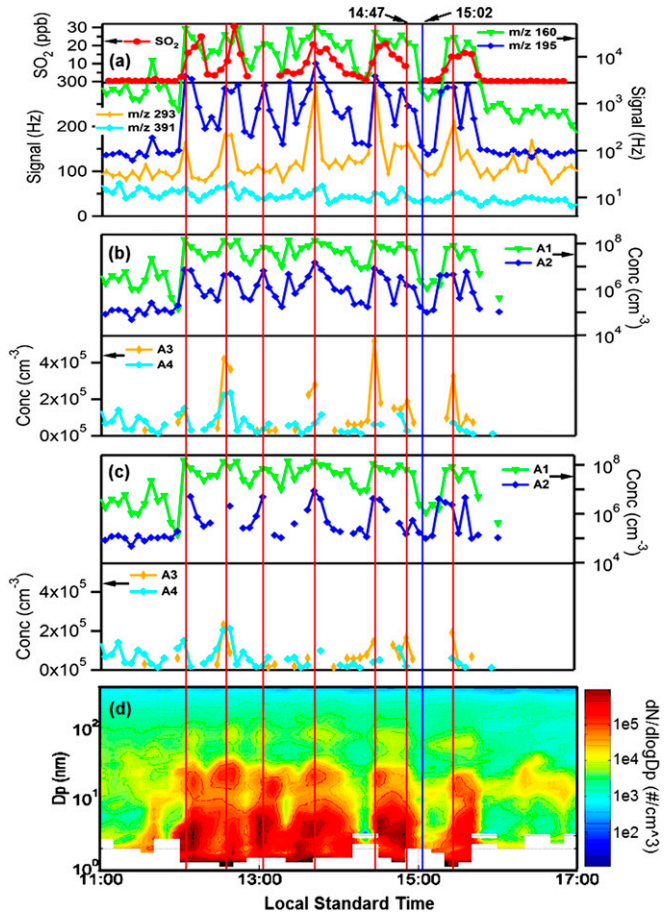

Fig. S5. Cluster CIMS, SO_2, and aerosol data on August 3, 2009. Details are provided in the *SI Text, Ambient Measurements with an Emphasis on Cluster CIMS Data*.

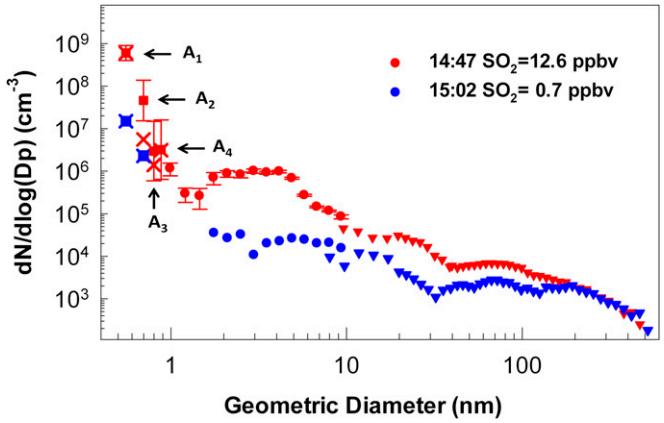

Fig. S6. Size distributions measured within (14:47) and outside (15:02) the plume at nearly the same time on August 3, 2009. Sulfuric acid monomer, dimer, trimer, and tetramer concentrations (■, effective rate IIC rate constants; X, collision rate IIC rate constants) and larger particles are all higher in the plume. (●) Measurements obtained with the DEG SMPS; ▼, measurements obtained using a pair of conventional mobility spectrometers. Trimer, tetramer, and 1–1.5-nm particles were below detection limits outside the plume.

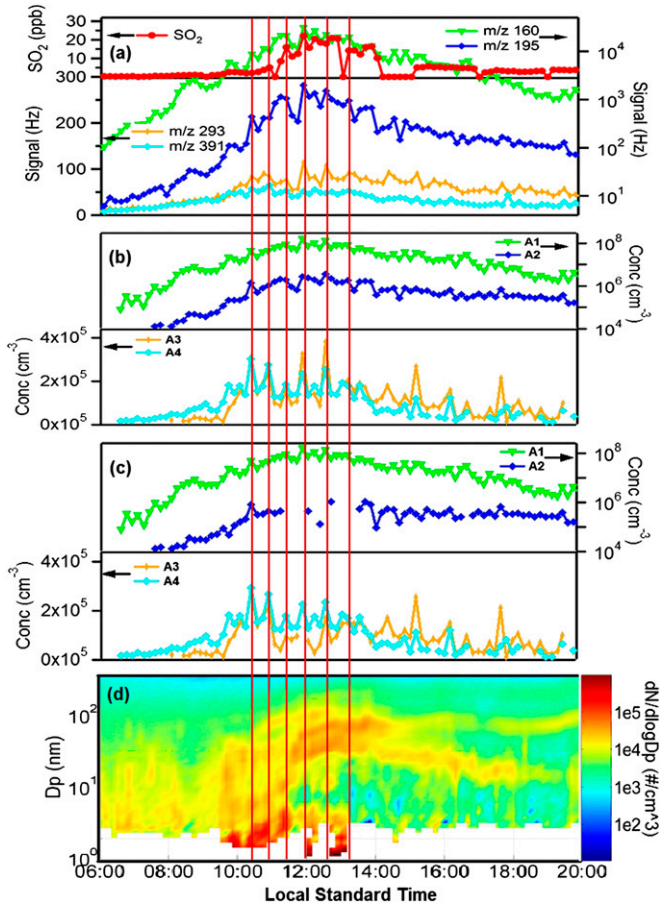

Fig. S7. Cluster CIMS, SO_2, and aerosol data on August 7, 2009. Details are provided in the *SI Text, Ambient Measurements with an Emphasis on Cluster CIMS Data*.

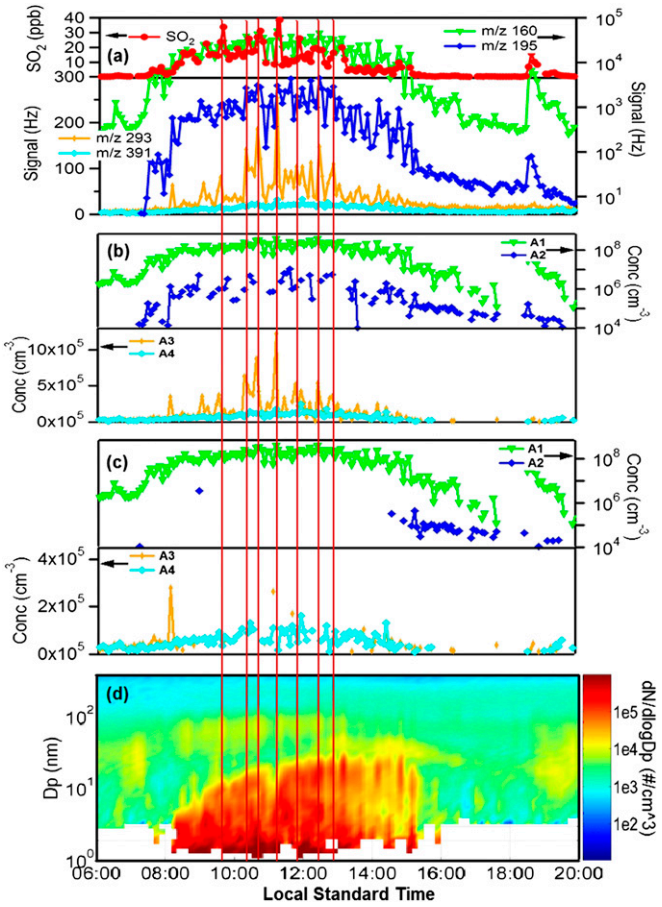

Fig. S8. Cluster CIMS, SO_2, and aerosol data on August 23, 2009. Details are provided in the *SI Text, Ambient Measurements with an Emphasis on Cluster CIMS Data*.

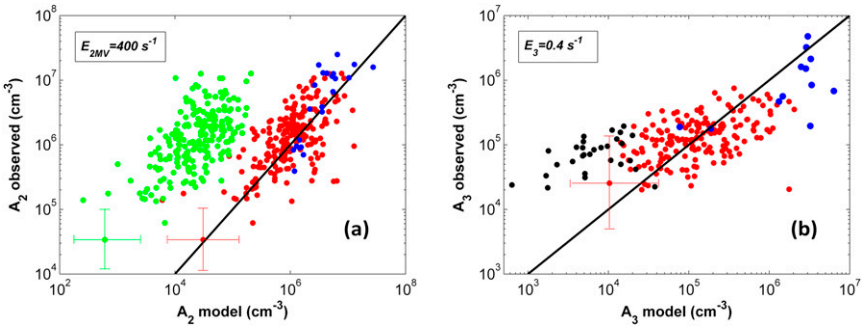

Fig. S9. Comparison of measured (vertical axes) and modeled (horizontal axes) concentrations of dimer (*A*) and trimer (*B*). Symbols shown in blue are from the chamber experiments and were obtained using the effective rate constants for IIC corrections. Other data (red, green, and black symbols) are from Atlanta (2009). For the red symbols in *A* it was assumed that [B] = ammonia plus amines, whereas for the green symbols [B] = total amines; ammonia concentrations were about 10 times higher than total amines. The black symbols in *B* were obtained when monomer concentrations were below 3×10^7 cm^{-3}. The 1:1 correlations are indicated by the diagonal black lines. The crosses, centered on randomly selected data points, apply to all data points and show estimated uncertainties in measured and modeled cluster concentrations.

Table S1. Sources of uncertainty in estimated cluster concentrations

Error source	Dimer	Trimer	Tetramer
Uncertainty in background correction ($R_{195.bkg}$,$R_{293.bkg}$,$R_{391.bkg}$)	±20%	±50%	±50%
Association rate constants	k_{21}: ±40%	k_{31}: ±70% k_{32}: ±70%	k_{41}: ±75% k_{42}: ±70% k_{43}: ±70%
Sulfuric acid monomer concentration		±30%	
Reaction time		±10%	
Mass-dependent sensitivity		±10%	
H_2SO_4 dissociation from clusters		0%	
Total estimated systematic uncertainty	2×	3×	3×